Interlocked chiral/polar domain walls and large optical rotation in Ni3TeO6

Xueyun Wang, Fei-Ting Huang, Junjie Yang, Yoon Seok Oh, and Sang-Wook Cheong

Citation: APL Materials **3**, 076105 (2015); doi: 10.1063/1.4927232
View online: http://dx.doi.org/10.1063/1.4927232
View Table of Contents: http://scitation.aip.org/content/aip/journal/aplmater/3/7?ver=pdfcov
Published by the AIP Publishing

Interlocked chiral/polar domain walls and large optical rotation in Ni_3TeO_6

Xueyun Wang,[1] Fei-Ting Huang,[1] Junjie Yang,[2,a] Yoon Seok Oh,[1,3] and Sang-Wook Cheong[1,2,b]

[1]*Rutgers Center for Emergent Materials and Department of Physics and Astronomy, Rutgers University, Piscataway, New Jersey 08854, USA*

[2]*Laboratory for Pohang Emergent Materials and Max Plank POSTECH Center for Complex Phase Materials, Pohang University of Science and Technology, Pohang 790-784, South Korea*

[3]*Department of Physics, Ulsan National Institute of Science and Technology (UNIST), Ulsan 689-798, South Korea*

(Received 1 May 2015; accepted 8 July 2015; published online 24 July 2015)

Chirality, i.e., handedness, pervades much of modern science from elementary particles, DNA-based biology to molecular chemistry; however, most of the chirality-relevant materials have been based on complex molecules. Here, we report inorganic single-crystalline Ni_3TeO_6, forming in a corundum-related $R3$ structure with both chirality and polarity. These chiral Ni_3TeO_6 single crystals exhibit a large optical specific rotation (α)—1355° dm^{-1} cm^3 g^{-1}. We demonstrate, for the first time, that in Ni_3TeO_6, chiral and polar domains form an intriguing domain pattern, resembling a radiation warning sign, which stems from interlocked chiral and polar domain walls through lowering of the wall energy. [http://dx.doi.org/10.1063/1.4927232]

Non-centrosymmetric materials are associated with important physical properties such as piezoelectricity, ferroelectricity, chirality, and non-linear optics, and relevant to numerous applications such as piezoelectric actuators, data storage devices, and electro-optical devices.[1–3] These non-centrosymmetric materials naturally accompany domains and domain walls that result from symmetry breaking away from centrosymmetry. Understanding and engineering of these domains and domain walls are quintessential for the technological utilization of these non-centrosymmetric materials.

Out of the crystallographic 32 point symmetry groups, 21 are non-centrosymmetric. Out of 21 non-centrosymmetric groups, 11 groups are chiral, 10 groups are polar, and five groups (1, 2, 3, 4, 6 in Hermann-Mauguin symbols) are simultaneously polar and chiral. Most investigations of chirality in material science have focused on molecule-based materials. There exist a significant number of chiral non-molecular materials.[3] However, the domain structures of these chiral inorganic materials have been studied only in a limited degree. Perhaps, the most well studied chiral domains in inorganic materials are those in chiral quartz (SiO_2; trigonal space group $P3_221$ or $P3_121$) — the so-called Dauphine twins.[4,5] Recently, chiral domains in $CsCuCl_3$ ($P6_122$ or $P6_522$) was studied using an imaging technique with circular polarized X-ray beams,[6] and quadrupole helix chirality of $DyFe_3(BO_3)_4$ ($P3_221$ or $P3_121$) was investigated using resonant X-ray diffraction.[7] The possible coupling between chiral and ferroelectric domains has been suggested in $Pb_5Ge_3O_{11}$ ($P3$).[8]

Sapphire (α-Al_2O_3) and Cr_2O_3 form in the centrosymmetric corundum crystallographic structure (space group R-3c). When antiferromagnetic order sets in Cr_2O_3, the magnetic lattice combined with the crystallographic lattice loses inversion symmetry, so Cr_2O_3 becomes linear magnetoelectric below the Néel temperature. $LiNbO_3$ forms in a modified corundum structure (space group $R3c$)

[a]Current address: Department of Physics, University of Virginia, Charlottesville, Virginia 22903, USA.
[b]Author to whom correspondence should be addressed. Electronic mail: sangc@physics.rutgers.edu.

with polarity, but no chirality. However, Ni_3TeO_6 crystallizes in a modified corundum structure (space group $R3$) with both chirality and polarity, and collinear antiferromagnetic order along the c-axis sets in below T_N = 52 K.[9,10] Chiral and polar domains and their relationship in Ni_3TeO_6 have never been studied previously.[11–14] In this letter, we report the relationship between chiral and polar domains in Ni_3TeO_6, and the large optical specific rotation in Ni_3TeO_6 associated with chirality.

Ni_3TeO_6 single crystals were grown using a chemical vapor transport method at 700 °C for 4 days, followed by furnace cooling.[9,10] Our Ni_3TeO_6 single crystals are transparent hexagonal plates ($\sim 1 \times 1 \times 0.1$ mm^3) with green color as shown in Fig. 1(c). Ni_3TeO_6 crystallizes in a chiral and polar lattice (space group $R3$) with lattice constants of a = 5.107 Å and c = 13.762 Å. In the corundum structure of α-Al_2O_3, edge-shared honeycomb layers of AlO_6 octahedra are stacked with an offset arrangement along the c-axis. In Ni_3TeO_6, both Ni and Te ions sit at the Al sites of corundum Al_2O_3 structure, leading to three crystallographically inequivalent Ni sites (labelled as

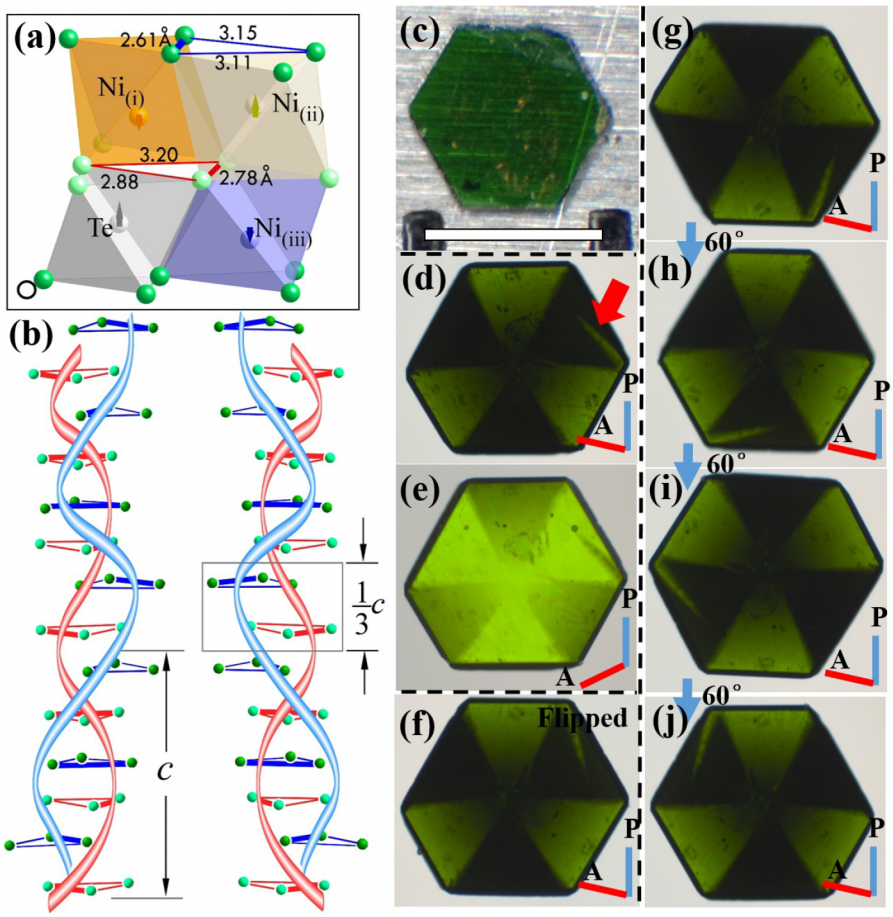

FIG. 1. (a) displays the basic building block of Ni_3TeO_6, which corresponds to one third of one unit cell. The red triangle is associated with unequal bond lengths: 2.78, 2.88, and 3.20 Å, which can be considered as a part of the first $Ni_{(iii)}O_6$-TeO_6 honeycomb layer. Then, the neighboring $Ni_{(i)}O_6$-$Ni_{(ii)}O_6$ layer is associated with the blue triangle with unequal bond lengths: 2.61, 3.11, and 3.15 Å. We denoted the shortest bonds in the red and blue triangles as bold lines. (b) shows two different ferri-chiral states: left panel with net left-handed chirality and right panel with net right-handed chirality. Red and blue helixes, shown by following the rotation of the bold red and blue bonds, respectively, rotate in an opposite fashion, and a net chirality exists due to the asymmetry of red and blue triangles (helices). (c) is an optical microscope image of a 100 μm-thick single crystal of Ni_3TeO_6: the scale bar equals to 1 mm. The chiral domains of a Ni_3TeO_6 crystal are visible in transmission polarized optical microscope images shown in Figs. [1(d)]–[1(j)]. Blue and red bars represent the angles of a polarizer and an analyzer, respectively. (d) and (e) show the contrast inversion of the chiral domains with rotating the analyzer from $\theta = 90° - \varphi$ to $90° + \varphi$. (f), compared with (d), shows no contrast change with flipping the crystal with a fixed polarizer/analyzer angle. (g)–(j) demonstrate no contrast change with in-plane rotation of the crystal with a fixed polarizer/analyzer angle (a red arrow labels one landmark which is an embedded different chiral domain, with which the crystal orientation can be identified).

$Ni_{(i)}$, $Ni_{(ii)}$, and $Ni_{(iii)}$) and one Te site.[11] Ni and Te ions occupy "3-fold" symmetry sites (Wyckoff position 3a, 0, 0, z) with z = 0.5065, 0.2144, 0.0127, and 0.7084 for $Ni_{(i)}$, $Ni_{(ii)}$, $Ni_{(iii)}$, and Te, respectively. Fig. 1(a) shows the first layer formed by an edge-shared network of $Ni_{(iii)}O_6$-TeO_6 octahedra, and another edge-shared network of $Ni_{(i)}O_6$-$Ni_{(ii)}O_6$ octahedra builds the second layer. As can be seen in Fig. 1(a), two layers are well connected via face-shared $Ni_{(ii)}O_6$-$Ni_{(iii)}O_6$ octahedra. Herein, we consider four of such oxygen bridged octahedra, $3NiO_6 + TeO_6$, as the basic building block of Ni_3TeO_6. Fig. S1 shows that three building blocks per unit cell are linked through interlayer stacking of TeO_6 and $Ni_{(i)}O_6$ octahedra via face sharing, resulting in a unique 120° rotation of neighboring building blocks (Section 1 in the supplementary material, see Fig. S1 for one unit cell consists of three $NiO_6 + TeO_6$ building blocks[15]).

To clarify the chirality of the Ni_3TeO_6 lattice, we define two oxygen triangles: red and blue triangles in Fig. 1(a), existing in the $Ni_{(iii)}O_6$-TeO_6 first layer and the $Ni_{(i)}O_6$-$Ni_{(ii)}O_6$ second layer, respectively. The red triangle in the first $Ni_{(iii)}O_6$-TeO_6 honeycomb layer is associated with three unequal bond lengths (2.78, 2.88, and 3.20 Å), and the neighboring $Ni_{(i)}O_6$-$Ni_{(ii)}O_6$ layer is characterized by the blue triangle with different three unequal bond lengths (2.61, 3.11, and 3.15 Å). The shortest bonds in red and blue triangles are highlighted in bold as shown in Fig. 1(a). The chiral structure is evident when tracking the red/blue triangles (or bold bonds) along the c axis, which reveals a 120° rotation of neighboring the-same-color triangles: three red triangles rotate counterclockwise (right-handed helix) about the c axis while the three blue triangles rotate clockwise (left-handed helix), as shown in Fig. 1(b). Note that these two helices have opposite chirality unlike the mono-chirality of double helix in DNA.[16] The opposite rotations are not cancelled in both x and y directions within one Ni_3TeO_6 unit cell due to different asymmetric triangles. The degree of chirality of a chiral structure can be quantified using a continuous chirality measure (CCM), obtained through finding the minimal distance, by which the atoms in the relevant structural fragment have to be shifted in order to reach the nearest achiral structure.[17,18] The concept of CCM was introduced to provide an exact quantitative scale of chirality, rather than labeling objects as being either chiral or achiral (Section 2 in the supplementary material, see Fig. S2(a) for the concept of CCM[15]). We obtain a CCM value for the blue helix which is two times larger than that of the red one. Thus, Ni_3TeO_6 forms a ferri-chiral state, i.e., the opposite chiral amplitude is unequal and a net chirality exists. Note that the ferri-chiral helices in Fig. 1(b) are winded and entangled around each other, and the CCM values of two helices are unequal, so the left panel in Fig. 1(b) shows an overall left-handed (L) chirality and the right panel is right-handed (R). The unique structural characteristic of Ni_3TeO_6 is the overall arrangement of hetero-helices of the octahedral building blocks, leading to its chirality. This is distinctly different from the corundum structure or the $LiNbO_3$ structure, which also exhibit similar two-types of helices, but two opposite helices accompany an identical CCM (i.e., red and blue triangles are identical in terms of bond lengths and angle). Therefore, they have no net chirality, so they are in an anti-chiral state (Section 2 in the supplementary material, see Fig. S2(b) for the comparison of corundum, $LiNbO_3$, and Ni_3TeO_6 structures[15]).

Unlike X-ray diffraction experiments using dispersion corrections or circularly polarized X-ray, measuring optical rotation with a polarized optical microscope is a relatively easy way to explore the chiral properties such as an optical specific rotation value. The chirality of a Ni_3TeO_6 single crystal has been directly observed under a transmission polarized optical microscope (Zeiss Optical Microscope Axio Imager, M1m). The blue and red bars in Figs. 1(d)-1(j) indicate the directions of a polarizer and an analyzer, respectively. It is clearly shown in Figs. 1(d) and 1(e) that by rotating the analyzer from $\theta = 90° - \varphi$ to $90° + \varphi$ (here, θ is the angle between the direction of polarizer and that of analyzer, and φ is a small additional rotation angle), the contrast of neighboring domains reverses. However, with a fixed $\theta = 90° - \varphi$, the domain contrast remains intact with flipping the crystal, as shown in Fig. 1(f). This is associated with an important feature of chirality: along either direction of a chiral helix, the chirality (i.e., left or right handedness) remains the same. Figs. 1(g)-1(j) demonstrate that in-plane rotation (the red arrow labels one landmark that enables the identification of crystal orientation readily) does not influence the domain contrast. Thus, the Ni_3TeO_6 crystal has six chiral domains with alternating left chiral and right chiral domains.

The chirality of a chiral crystal can be characterized by an optical specific rotation value: $\alpha = \varphi/ld$, where φ is the optical rotation angle, l is the path length in decimeter, and d is the

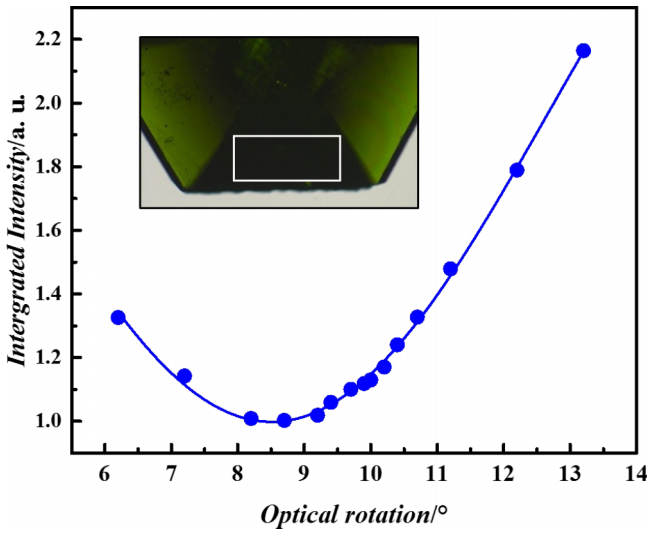

FIG. 2. Shows the dependence of the integrated intensity of linearly polarized light passed through a Ni_3TeO_6 crystal on analyzer angle, indicating that at $\varphi = 8.5°$, the integrated light intensity reaches the minimum. The plot is fitted by $I \propto \cos^2 \varphi$.

density of crystal. The optical rotation of a Ni_3TeO_6 crystal is carefully measured using an optical microscope with linear-polarized visible light in a transmission mode. Fig. 2 shows the dependence of integrated light intensity on analyzer angle. At $\varphi = 8.5°$, the integrated light intensity (I) reaches the minimum, meaning that the analyzer is exactly perpendicular to the rotated linearly polarized light passed through the crystal. The plot can be nicely fitted by $I \propto \cos^2 \varphi$. The crystal thickness is 9.8×10^{-4} dm, and the density of Ni_3TeO_6 is 6.4 g cm^{-3}.[19] Thus, the measured specific rotation of Ni_3TeO_6 is 1355° dm^{-1} cm^3 g^{-1} in a visible frequency range, which is about twice larger than that of α-quartz. A list of the specific rotations of various inorganic chiral materials is shown in Table I, which is calculated based on Refs. 8 and 20.

In addition to chirality, the imbalanced spatial charge distributions of the ions in Ni_3TeO_6 give rise to electric polarization along the c axis. Thus, Ni_3TeO_6 is a rather unique material with chirality and polarity at room temperature. Both polar distortions along [001] and chiral distortions around [001] are involved in forming the $R3$ rhombohedral structure of Ni_3TeO_6. With respect to the zero polarization when the polar mode is deactivated, the polarization of the $R3$ rhombohedral structure of Ni_3TeO_6 is 72 μC cm^{-2}.[11] Piezoresponse force Microscopy (PFM) scanning experiment was performed on the flat surface of a Ni_3TeO_6 crystal using an atomic force microscope (Nanoscope IIIA). The top panel of Fig. 3(c) shows the topography of the purple boxed region across one chiral domain wall in Fig. 3(a), and the corresponding out-of-plane PFM image is shown in the middle panel of Fig. 3(c). The contrast of the PFM image results from the opposite piezoresponse signal in adjacent chiral domains, indicating the the presence of opposite c-direction polarizations (up (+) or down (−)) in two adjacent chiral domains. We attempted to flip polarization with external electric fields without success, indicating that Ni_3TeO_6 is pyroelectric (see Section 3 in the supplementary material[15]). Note that there exist 4 different possibilities of combining chirality (R or L) and polarization directions

TABLE I. Specific rotation (α) of inorganic chiral materials.

Compounds	α (deg dm^{-1} cm^3 g^{-1})	Compounds	α (deg dm^{-1} cm^3 g^{-1})
$AgGaS_2$	11 397	Ni_3TeO_6	1355
$Hg_3Te_2Cl_2$	5 270	HIO_3	1089
$LiIO_3$	2 200	SiO_2 (α-quartz)	816
TeO_2	1 852	$Bi_{12}GeO_{20}$	438
HgS	1 636	$Pb_5Ge_3O_{11}$	80

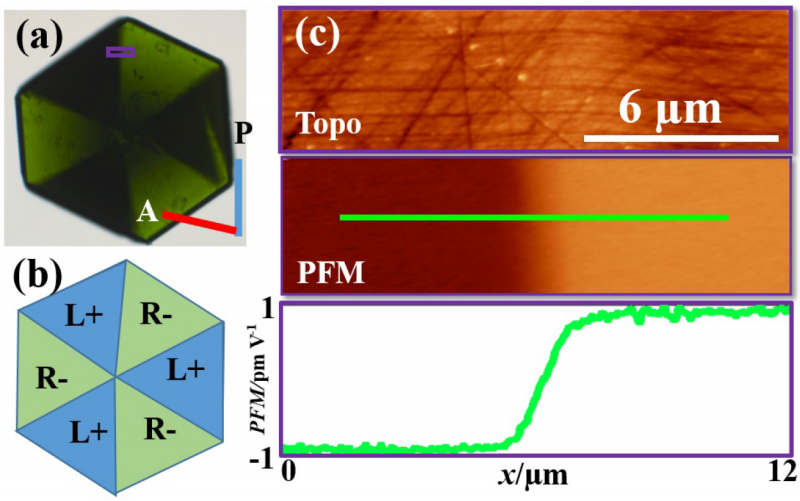

FIG. 3. Demonstrates that a chiral domain wall is also a polar domain wall. PFM image of the purple boxed region in the transmission polarized optical microscope image of (a) is shown in the middle panel of (c). The corresponding topographic image is displayed in the top panel of (c), and the line-scan along the green line is shown in the bottom panel of (c). The cartoon in (b) displays one possible domain structure with (R−, L+, R−, L+, R−, L+).

(+ or −). However, our results indicate that the 6 domain structure of a Ni_3TeO_6 crystal is either (R+, L−, R+, L−, R+, L−) or (R−, L+, R−, L+, R−, L+), one of which is shown in the cartoon in Fig. 3(b). In other words, chiral domain walls are interlocked with polar domain walls.

Fig. 4(a) shows the top view of the structure including one-building-block around one chiral domain wall of Ni_3TeO_6, and the corresponding schematic side view is displayed in Fig. 4(b). The off-centered cations, $Te/Ni_{(ii)}$ and $Ni_{(i)}/Ni_{(iii)}$, show opposite displacements along the polar direction. Te and $Ni_{(ii)}$ ions, in comparison with $Ni_{(i)}$ and $Ni_{(iii)}$ ions, exhibit larger displacements along the *c* axis from the center of oxygen atoms. The up-polar state is associated with the upward shift of Te and $Ni_{(ii)}$ ions from the octahedral centers. Correspondingly, the downward-polar state forms when Te and $Ni_{(ii)}$ ions shift down from the octahedral centers. For example, the left domain shown in Figs. 4(a) and 4(b) represents an up-polar and left-handed (L+) domain. For convenience, a cation sitting at *i*th layer and one of A, B, and C columns is denoted as M_i (M = A/B/C and i = 1-6). For example, the staggered stacking sequence of TeO_6 in the left domain of Fig. 4(b) corresponds to $A_1B_3C_5$.

Figs. 4(b)-4(d) display three types of structural domain walls: chiral-only domain wall (c), polar-only domain wall (d), and simultaneous chiral and polar domain wall (b). First, Fig. 4(c) shows the chiral-only domain wall between L+ and R+, at which mirror symmetry with respect to the (10-10) plane exists. The polarity does not change across this chiral domain wall, but the rotational feature of three building blocks is switched across the chiral domain wall. Second, cations are displaced in the opposite direction across the polar domain wall between L+ and L− in Fig. 4(d) while chirality remains intact. The TeO_6 octahedra in both Figs. 4(c) and 4(d) show an $A_1B_3C_5||A_1B_5C_3$ sequence across the domain walls, so the continuity of the ideal TeO_6 octahedra stacking sequence is broken across the wall. On the other hand, across the simultaneous chiral and polar domain wall in Fig. 4(b), the ideal $A_1B_3C_5$ stacking of TeO_6 octahedra remains intact. Thus, simultaneous chiral and polar domain walls, compared with chiral-only or polar-only walls, likely accompany low domain wall energy, which leads to the interlocking of chiral and polar domain walls. This interlocking of chiral and polar domain walls is basically responsible for the intriguing radiation warning sign-like pattern in a hexagonal-shape Ni_3TeO_6 crystal. Our findings demonstrate, for the first time, the interlocking nature of chiral and polar domain walls in any inorganic materials. Note that the coupling or coexistence of different order parameters gives rise to novel unconventional properties such as multiferroicity,[21,22] improper ferroelectricity,[23–26] and anomalous magnetotransport.[22,27] Similarly, the study of the coupling between chiral and polar domains and

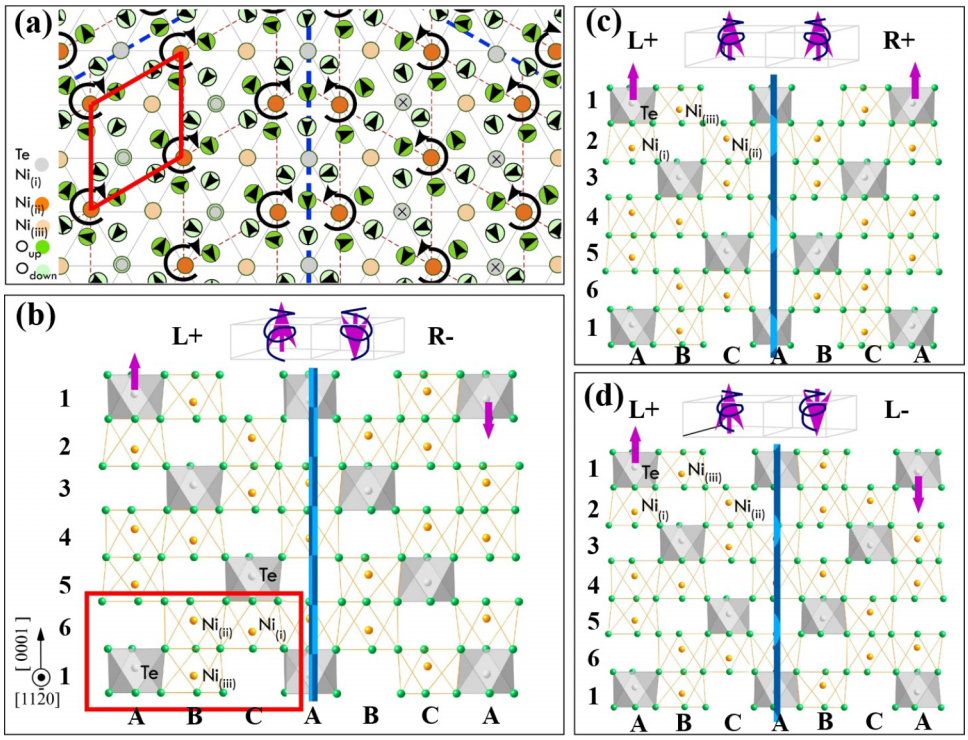

FIG. 4. Three types of structural domains and domain walls in Ni_3TeO_6. (a) and (b) show the top view and side view of a simultaneous chiral and polar domain wall. The thickness of the structure along the *c* axis in (a) is one-building-block, corresponding to the red rectangular frame in (b). (c) and (d) display a chiral-only domain wall between R+ and L+ domains, and a polar-only domain wall between L+ and L− domains, respectively. The Te stacking sequence remains intact across a domain wall only in (b) while it switches in (c) and (d).

domain walls may provide new paths for understanding the novel physical properties of chiral and polar materials and utilizing them for technological applications.

In summary, we have successfully grown transparent hexagonal single crystals of Ni_3TeO_6, which crystallizes in a corundum-related structure. Unlike other compounds with corundum-related structures such as α-Al_2O_3, Cr_2O_3, and $LiNbO_3$, Ni_3TeO_6 exhibits uniquely both chirality and polarity with a large optical specific rotation (α = 1355° dm^{-1} cm^3 g^{-1}), which may be utilized for devices such as polarization rotators.[28] Note that most inorganic materials listed in Table I showing large specific rotation value possess merely chirality without polarity. In addition, our results demonstrate that the interlocked chiral and polar domain walls can minimize lattice distortions at the walls and lead to a unique radiation warning sign-like domain pattern in Ni_3TeO_6. Our findings unveil the rich coupling nature of chiral and polar order parameters and provide new insights into understanding and engineering of domains and domain walls in functional chiral and polar materials, which have been investigated only in a limited degree.

We thank D. Vanderbilt and Jan Musfeldt for stimulating discussion. The work at Rutgers is supported by the Gordon and Betty Moore Foundation's EPiQS Initiative through Grant No. GBMF4413 to the Rutgers Center for Emergent Materials. The work at Postech is supported by the Max Planck POSTECH/KOREA Research Initiative Program [Grant No. 2011-0031558] through NRF of Korea funded by MEST. Y.S.O. is supported in part by the year of 2014 Research Fund (No. 1.140081.01) of the UNIST (Ulsan National Institute of Science and Technology).

[1] J. X. Zhang, R. J. Zeches, Q. He, Y. H. Chu, and R. Ramesh, Nanoscale **4**(20), 6196–6204 (2012).
[2] C. Chappert, A. Fert, and F. N. Van Dau, Nat. Mater. **6**(11), 813–823 (2007).
[3] P. S. Halasyamani and K. R. Poeppelmeier, Chem. Mater. **10**(10), 2753–2769 (1998).
[4] Y. Tanaka, T. Kojima, Y. Takata, A. Chainani, S. W. Lovesey, K. S. Knight, T. Takeuchi, M. Oura, Y. Senba, H. Ohashi, and S. Shin, Phys. Rev. B **81**(14), 9 (2010).
[5] J. Igarashi and M. Takahashi, Phys. Rev. B **86**(10), 10 (2012).

[6] H. Ohsumi, A. Tokuda, S. Takeshita, M. Takata, M. Suzuki, N. Kawamura, Y. Kousaka, J. Akimitsu, and T.-H. Arima, Angew. Chem., Int. Ed. **52**(33), 8718–8721 (2013).
[7] T. Usui, Y. Tanaka, H. Nakajima, M. Taguchi, A. Chainani, M. Oura, S. Shin, N. Katayama, H. Sawa, Y. Wakabayashi, and T. Kimura, Nat. Mater. **13**(6), 611–618 (2014).
[8] J. P. Dougherty, E. Sawaguchi, and L. E. Cross, Appl. Phys. Lett. **20**(9), 364–365 (1972).
[9] Y. S. Oh, S. Artyukhin, J. J. Yang, V. Zapf, J. W. Kim, D. Vanderbilt, and S. W. Cheong, Nat. Commun. **5**, 3201 (2014).
[10] I. Zivkovic, K. Prsa, O. Zaharko, and H. Berger, J. Phys.: Condens. Matter **22**(5), 056002 (2010).
[11] R. Becker and H. Berger, Acta Crystallogr., Sect. E: Struct. Rep. Online **62**, I222–I223 (2006).
[12] F. Wu, E. Kan, C. A. Tian, and M. H. Whangbo, Inorg. Chem. **49**(16), 7545–7548 (2010).
[13] R. Mathieu, S. A. Ivanov, P. Nordblad, and M. Weil, Eur. Phys. J. B **86**(8), 4 (2013).
[14] R. Sankar, G. J. Shu, B. K. Moorthy, R. Jayavel, and F. C. Chou, Dalton Trans. **42**(29), 10439–10443 (2013).
[15] See supplementary material at http://dx.doi.org/10.1063/1.4927232 for details of unit cell and concept of CCM.
[16] J. D. Watson and G. S. Stent, *Double Helix* (Simon and Schuster, 1998).
[17] H. Zabrodsky and D. Avnir, J. Am. Chem. Soc. **117**(1), 462–473 (1995).
[18] See http://www.csm.huji.ac.il/new/index.php for online calculation of CCM value.
[19] P. Villars, K. Cenzual, J. Daams, R. Gladyshevskii, O. Shcherban, V. Dubenskyy, V. Kuprysyuk, and I. Savysyuk, in *Structure Types. Part 9: Space Groups (148) R-3-(141) I41/amd*, edited by P. Villars and K. Cenzual (Springer, Berlin, Heidelberg, 2010), Vol. 43A9, p. 345.
[20] J. Jerphagnon and D. S. Chemla, J. Chem. Phys. **65**(4), 1522–1529 (1976).
[21] S.-W. Cheong and M. Mostovoy, Nat. Mater. **6**(1), 13–20 (2007).
[22] T. Kimura, Annu. Rev. Mater. Res. **37**, 387–413 (2007).
[23] C. J. Fennie and K. M. Rabe, Phys. Rev. B **72**(10), 100103 (2005).
[24] T. Choi, Y. Horibe, H. T. Yi, Y. J. Choi, W. Wu, and S. W. Cheong, Nat. Mater. **9**(3), 253–258 (2010).
[25] N. A. Benedek and C. J. Fennie, Phys. Rev. Lett. **106**(10), 107204 (2011).
[26] Y. S. Oh, X. Luo, F.-T. Huang, Y. Wang, and S.-W. Cheong, Nat. Mater. **14**(4), 407–413 (2015).
[27] N. Nagaosa, J. Sinova, S. Onoda, A. H. MacDonald, and N. P. Ong, Rev. Mod. Phys. **82**(2), 1539–1592 (2010).
[28] D. H. Kwon and D. H. Werner, Opt. Express **16**(23), 18731–18738 (2008).